

# New X-ray views of the Galactic center observed with *Suzaku*

Katsuji Koyama, Yoshiaki Hyodo and Tatsuya Inui

Department of Physics, Graduate school of Science, Kyoto University, Sakyo-ku, Kyoto  
606-8502

E-mail: koyama@cr.scphys.kyoto-u.ac.jp

## Abstract.

We report the diffuse X-ray emissions from the Sgr A and B regions observed with *Suzaku*. From the Sgr A region, we found many K-shell transition lines of iron and nickel. The brightest are  $K\alpha$  lines from FeI, FeXXV and FeXXVI at 6.4 keV, 6.7 keV and 6.9 keV. In addition,  $K\alpha$  lines of NiI and NiXXVII,  $K\beta$  of FeI, FeXXV and FeXXVI, and  $K\gamma$  of FeXXV and FeXXVI are detected for the first time. The center energy of  $K\alpha$  of FeXXV favors collisional excitation as the origin for this line emission. The ionization temperature determined from the flux ratio of  $K\alpha$  of FeXXV and FeXXVI is similar to the electron temperature determined from the flux ratio of  $K\alpha$  and  $K\beta$  of FeXXV, which are in the range of 5–7 keV. Consequently, the Galactic Center diffuse X-rays (GCDX) are consistent with emission from a plasma nearly in ionization equilibrium. The radio complex Sgr B region also exhibits  $K\alpha$  lines of FeI, FeXXV and FeXXVI. The 6.7 keV line (FeXXV) map exhibits a local excess at  $(l, b) = (0^\circ.612, 0^\circ.01)$ , and could be a new young SNR. The 6.4 keV image is clumpy with local excesses near Sgr B2 and at  $(l, b) = (0^\circ.74, -0^\circ.09)$ . Like Sgr B2, this latter excess may be another X-ray reflection Nebulae (XRN).

## 1. Introduction

The *AstroE2* satellite was launched on 10th July in 2005 and was named *Suzaku* [1] after an imaginary red bird in the ancient oriental mythology. The X-ray Imaging Spectrometer (XIS) [2] is one of the major instruments on *Suzaku*. The XIS consists of four sets of X-ray CCD cameras, placed on the focal planes of the X-ray Telescope (XRT) [3]. Three XIS sensors contain front-illuminated (FI) CCDs, and the other has a back-illuminated (BI) CCD [2]. The other focal plane instrument is the micro-calorimeter (XRS) [4], which had extremely high energy resolution. The XRS was cooled down to 60 mK, and its overall energy resolution was originally 7 eV at 5.9 keV. These temperature and energy resolution were on-orbit world records. The XRS was able to resolve, e. g., the iron He-like triplets, and hence should have opened a new window of X-ray astronomy. However, regretfully, all the liquid He evaporated very quickly. We nevertheless still have the XIS, which have the best performances among space CCD cameras. The background level for diffuse sources, in particular at the energy of 5–10 keV range is nearly one order of magnitude lower than *Chandra* and *XMM*. The effective area and energy resolution are also comparable to or better than *XMM*. Therefore the XIS on *Suzaku* is best suited for observations of the diffuse X-rays from the Galactic Center (GC). Early *Suzaku* results will appear soon in the refereed journal ([5], [6]). This paper reports the summary and

essence of these papers.

## 2. The Sgr A Region

We have made narrow band GC maps in the 6.34–6.46 keV and 6.62–6.74 keV bands, which are shown in figures 1 and 2. Although these line energies are very close to each other, the X-ray maps are entirely different. The 6.4 keV line is the  $K\alpha$  of FeI, hence figure 1 traces molecular clouds. While the 6.7 keV line is  $K\alpha$  of FeXXV, hence figure 2 traces very hot plasma.

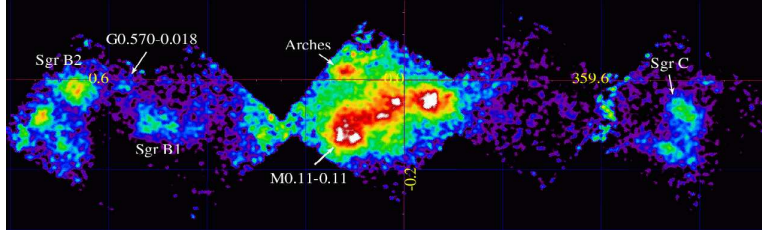


**Figure 1.** The narrow band map at the 6.4 keV line (the 6.34–6.46 keV band). Coordinates are galactic  $l$  and  $b$  in degrees.

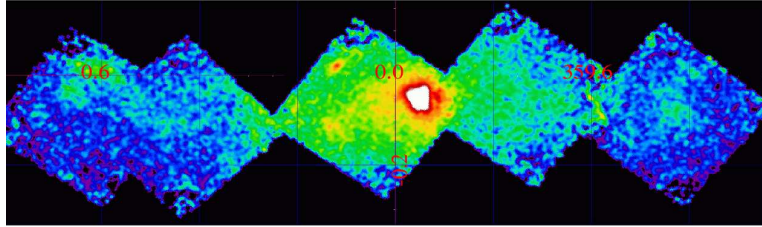


**Figure 2.** Same as figure 1, but for the 6.7 keV line (the 6.62–6.74 keV band).

**Table 1.** The detected lines from the Sgr A region.

Emission lines	
Observed Center Energy* (eV)	Identification Line
6409	FeI $K\alpha$
6680	FeXXV $K\alpha$
6969	FeXXVI $Ly\alpha$
7069	FeI $K\beta$
7490	NiI $K\alpha$
7781	NiXXVII $K\alpha$
7891	FeXXV $K\beta$
8220	FeXXVI $Ly\beta$
8264	FeXXV $K\gamma$
8681	FeXXVI $Ly\gamma$

\* systematic line error is  ${}^{+2}_{-7}$  eV.

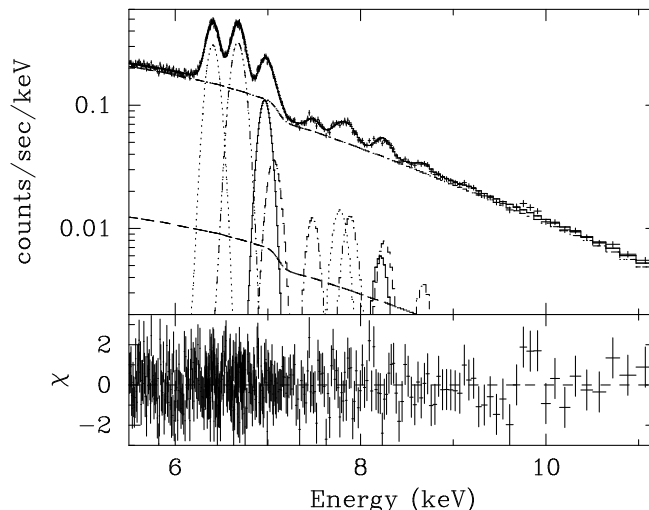


**Figure 3.** The averaged spectrum of the 3 FIs in the 5.5–11.5 keV band. The data are taken from the full FOV excluding the calibration source regions and Sgr A East. The best-fit result is shown with the dot-dashed line. The long-dashed line is the model of the cosmic X-ray background (CXB) (after Koyama et al. 2006b, *PASJ*, submitted).

### 2.1. The center energy and width of $K\alpha$ line of FeXXV

The spectrum of the GCDX from the three FIs is given in figure 3, where the non X-ray background (NXBG) made from the night earth data is subtracted. We fit the spectrum with a phenomenological model (thermal bremsstrahlung + Gaussians + absorption edge). The best-fit line center energies and the best line candidates are given in table 1, where the possible systematic errors of the line center energies are  ${}_{-7}^{+2}$  eV. The center energy of  $K\alpha$  of FeXXV is  $6680 \pm 1$  eV. This line is a blend of resonance, inter-combination and forbidden lines, hence the energy depends on the flux ratio of these 3 lines.

For the origin of  $K\alpha$  lines of FeXXV and FeXXVI, we discuss two possible cases: (1) collisional ionization and (2) recombining plasma, while the latter case (case 2) includes a photo-ionized plasma and charge exchange processes. The most distinct difference between the two cases is the flux ratio of resonance and forbidden lines, such that collisional ionizing plasma (1) emits the stronger resonance line than the forbidden line by factor of 2, and vice versa for the recombining plasma (2). In fact, the *Chandra* and *XMM-Newton* grating data of many stellar coronae (case 1) have confirmed the relative dominance of the resonance line in comparison to the forbidden line. On the other hand, the case 2, the recombining of a low temperature electron is seen in a photo-ionized plasma, with the typical case being NGC 1068 [7], which shows a larger flux of the forbidden line than that of the resonance line. Thus the center energy of  $K\alpha$  of FeXXV should be different for the two cases.

The center energy of the collisional ionization plasma (1) and that of the charge exchange process (2) were measured from the iron ion beam experiment in the laboratory [8]). The center energy depends on the energy of iron beam and target materials. Within a reasonable range of conditions, the collisional ionization plasma (1) and the charge exchange process (2) give center energies of 6680–6685 eV and 6666 eV, respectively. We also simulated the collisional-ionization case using the plasma codes APEC and MEKAL, and also find central energies of 6680 eV (MEKAL) and 6685 eV (APEC), respectively. Our observed energy of 6680 eV agrees well with collisional ionization plasma of the laboratory data and the MEKAL model, or at most, differ only 5 eV from the APEC model. The line width ( $1\sigma$ ) of  $K\alpha$  of FeXXV is determined

to be 38 eV, exceeding the systematic effect of  $\sim 30$  eV (the width of the calibration line). This large line broadening would be due mainly to the triplet lines and satellite lines.

### 2.2. Constraints on the cosmic ray iron velocity in the charge exchange scenario

The other constraint on the charge exchange process is the Lyman limit hump. If an electron is captured to a level of a large principal quantum number of an iron nucleus, the subsequent decay to the ground state produces a hump at Lyman series limit ( $\sim 9.2$  keV). However we see no significant hump with the upper limit of  $9 \times 10^{-6}$  photons  $\text{s}^{-1} \text{cm}^{-2}$  (we assumed a Gaussian line with width 30 eV), which is about 6% of the intensity of  $\text{Ly}\alpha$ . This upper limit sets the lower limit of the collision energy to  $> 100$  eV  $\text{amu}^{-1}$  [9], [10]. Thus the velocity of bare iron nuclei must be larger than  $\sim 150$  km  $\text{s}^{-1}$ , or the line width of  $\text{K}\alpha$  of FeXXVI ( $\text{Ly}\alpha$ ) must be larger than 3 eV. Since the observed line width is smaller than that of the calibration line, the real line broadening should be nearly zero. This is inconsistent with no hump at 9.2 keV. We however note that the accurate measurement of the line broadening of this level ( $\sim 3$  eV) is very difficult with the XIS, hence further confirmation with better resolution instruments is very important.

Together with the discussion of the previous section, we conclude that the 6.7 keV and 6.9 keV lines in the GCDX are caused by collisional ionization and do not originate from the charge exchange process.

### 2.3. The flux ratio of K-shell transition lines of FeXXV, XXVI and NiXXVII

The ionization temperature determined from the best-fit  $\text{K}\alpha$  flux ratio between FeXXVI and FeXXV is similar to the electron temperature determined from the best-fit flux ratio of  $\text{K}\beta$  and  $\text{K}\alpha$  of FeXXV, within the error range of 5–7 keV. The observed flux ratios of  $\text{K}\beta$  and  $\text{K}\alpha$  of FeXXVI, and  $\text{K}\gamma$  and  $\text{K}\alpha$  of FeXXV, XXVI are all consistent with an electron temperature of  $\sim 5 - 7$  keV. With the assumption that the relative abundances of iron and nickel are proportional to the solar value, the  $\text{K}\alpha$  ratio between NiXXVII and FeXXV is consistent with an the ionization temperature of  $\sim 5$  keV. We therefore conclude that the temperature of the GC is  $\sim 5 - 7$  keV in collisional ionization equilibrium.

## 3. The Sgr B Region

The X-ray spectrum of all the Sgr B region is given in figure 4. The spectra of the four XISs (XIS0-XIS3) are co-added and the NXBG is subtracted. With the superior energy resolution of the XIS for diffuse sources, we can clearly resolve the 6.4 keV, 6.7 keV and 6.9 keV lines.

In order to study this region more quantitatively, we have divided the XIS FOV into 16 ( $4 \times 4$ ) areas as is shown in figure 5 by the solid grids. For brevity, we assign coordinates for each square position such as (0, 0) and (3, 3), where the former and latter are lower-left and upper-right positions, respectively. Since the satellite roll-angle of the observation was nearly  $0^\circ$ , the north of this coordinate is also the north of the sky coordinate. The four corners, (0, 0), (0, 3), (3, 0) and (3, 3) contain the MnI  $\text{K}\alpha$  and  $\text{K}\beta$  line from the built-in calibration sources, so we exclude these 4 areas in the following analysis.

We then made X-ray spectra from the 12 squares. The NXBG spectra are constructed from night earth data in the same detector area of the 12-square regions and subtracted from the spectra of the 12 Sgr B regions. The NXBG-subtracted spectra are fitted with a model of thermal bremsstrahlung plus Fe absorption edge at the 7.1 keV and four emission lines, which are the  $\text{K}\alpha$  lines from FeI (6.4 keV), FeXXV (6.7 keV) and FeXXVI (6.9 keV) and the  $\text{K}\beta$  line from FeI (7.06 keV). Using the best-fit fluxes, we made color code maps (figure 5), which are the fluxes of 6.4 keV (figure 5a), 6.7 keV (5b), the flux ratio of 6.9 keV/6.7 keV (5c), and the continuum flux (5d).

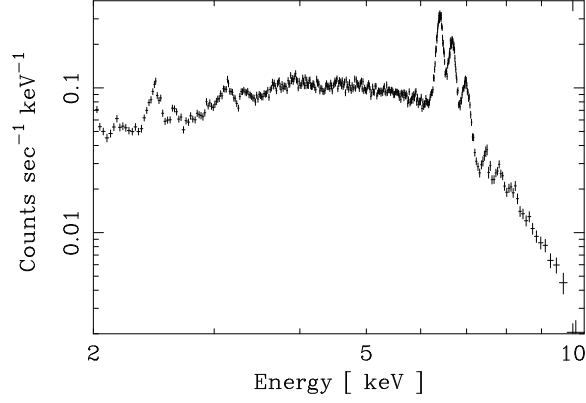


**Figure 4.** The X-ray spectra from the full FOV of the XIS, but the CCD corners irradiated by the build-in calibration sources are excluded. All the four XIS data are co-added

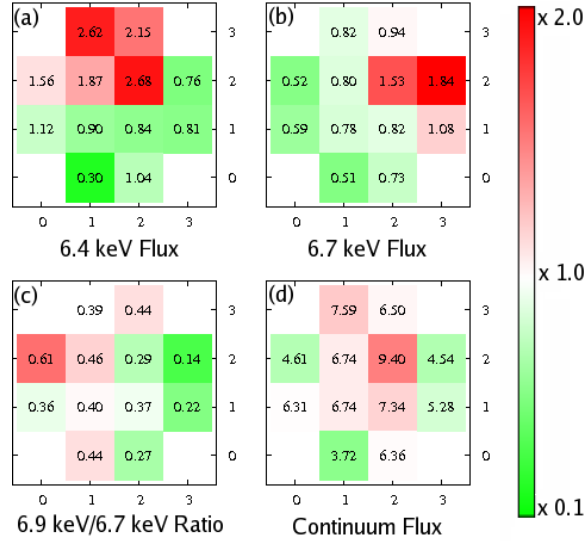


**Figure 5.** The 6.4 keV (a), 6.7 keV (b), the flux ratio of 6.9 keV/6.7 keV (c), and the continuum flux map (d). The embedded numbers are fluxes in units of  $10^{-5}$  photons  $\text{cm}^{-2}$   $\text{s}^{-1}$   $\text{arcmin}^{-2}$  or flux ratios. The color means that the average value is white, and the increasing (decreasing) excess above (below) the average is given with increasing deepness of red (green), where the maximum (minimum) is 2.0 (0.1) times of the average value.

Both the 6.4 and 6.7 keV line maps show a large contrast in red and green colors, which means that the fluxes have large variation from position to position. On the other hand, the 6.9 keV/6.7 keV ratio is rather smooth (the contrast of colors is weak) except the positions of (3, 2) and (0, 2). If we exclude these positions, the mean value of the other 10 squares is 0.36. For a plasma in collisional ionization equilibrium (CIE), this value corresponds to a temperature of 6–7 keV. Koyama et al. (2006b) reported that the mean temperature of the Galactic Center diffuse X-ray emission (GCDX) is 5–7 keV. We thus conclude that the origin of the diffuse emission is the same. At the Sgr B region, the surface brightness of the GCDX is about a half of that in Sgr A.

The significant excess of the 6.7 keV flux and deficit of the 6.9 keV/6.7 keV flux ratio at

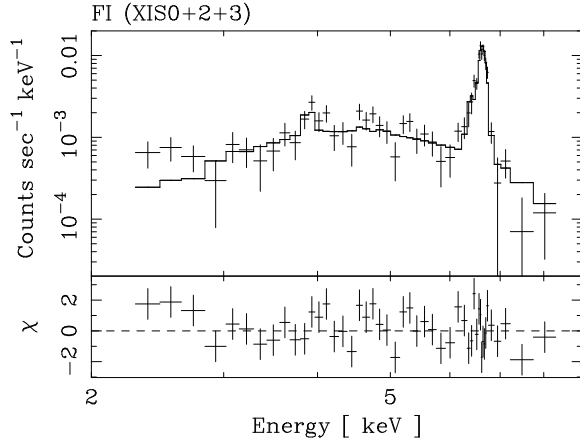


**Figure 6.** The X-ray spectrum of the sum of 3 FI CCDs for a new SNR (G0.61+0.01) with the best-fit VNEI model (after Koyama et al. 2006c, *PASJ*, submitted).

the position of (3, 2) indicates that an extra component with strong 6.7 keV line but no strong 6.9 keV line is present at this position. The rather smooth distribution of the continuum X-ray fluxes (see figure 5d) also suggests that the excess emission is mainly due to the 6.7 keV line. Since the 6.7 keV line is most likely the  $K\alpha$  of FeXXV, a probable origin of the local 6.7 keV excess is a hot plasma with a temperature lower than the large scale GCDX. The 6.9 keV/6.7 keV flux ratio at the position (3, 2) is 0.14, which can be converted to an ionization temperature of  $\sim 4$ –5 keV. This temperature is typical for a young SNR like Sgr A East. The 6.4 keV flux (figure 5a) shows local excesses at the position of Sgr B2 (2, 2) and the east of Sgr B2 (1, 3). The presence of the 6.4 keV line is strong evidence for dense and cool molecular clouds.

### 3.1. Discovery of a new young SNR

Since the 6.7 keV excess at the position of (3, 2) is likely to be a new SNR (see discussion below), we designate this source as Suzaku J1747.0-2824.5 (G0.61+0.01) from its center position. The background-subtracted spectrum of G0.61+0.01 is given in figure 6, for the 3 FIs case, where the background was taken from the southeast region. We see pronounced peak at 6.7 keV, but the line shape is asymmetric with a tail at lower energy. This tail would be due to the presence of a faint  $K\alpha$  line of FeI at 6.4 keV.

The FI and BI spectra are simultaneously fitted with a thin thermal plasma in non-equilibrium ionization (VNEI) [11], adding two Gaussian lines at 6.4 keV and 7.06 keV. These two lines represent the  $K\alpha$  and  $K\beta$  lines of FeI, where the flux of latter line is fixed to 12.5% of the former. The best-fit result for the FI is shown in figure 6. The best-fit temperature is  $\sim 3$  keV and the abundances of Ca and Fe are 3–4 times of solar. The  $N_{\text{H}}$  value is  $1.6 \times 10^{23} \text{ cm}^{-2}$ , larger than the typical value to the GC ( $6 \times 10^{22} \text{ H cm}^{-2}$ ) [12]. Therefore, G0.61+0.01 would be located behind or in the rim of the Sgr B2 cloud. Since G0.61+0.01 is located in the south of an expanding radio shell [13], which is probably interacting with the Sgr B2 cloud rim, we assume that the distance of G0.61+0.01 is the same as Sgr B2 and to be 8.5 kpc [14]. Then the G0.61+0.01 size of about 2.4 arcmin (the radius of the major axis) corresponds the real size of 6 pc. Dividing this size by the sound velocity of the 3 keV plasma, we obtain the dynamical time scale of  $\sim 4 \times 10^3$  years. The 2–10 keV band luminosity is estimated to be  $1.5 \times 10^{34} \text{ ergs s}^{-1}$ . These values are typical for an ejecta dominated young SNR.

Since G0.61+0.01 is found at the edge of the XIS field, some parts of this candidate SNR would be out of the XIS field. One possibility is that G0.61+0.01 is a part of the expanding

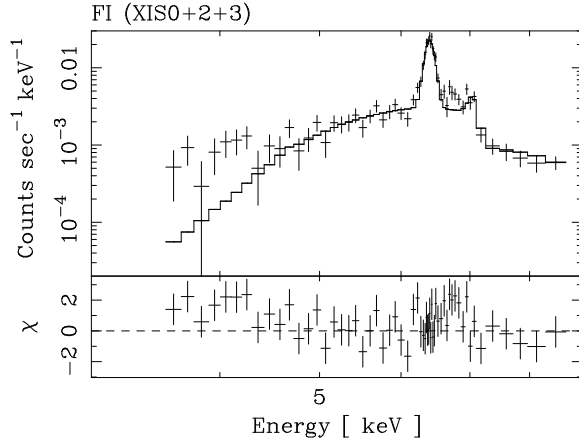


**Figure 7.** The X-ray spectrum of the sum of the 3 FI CCDs for Sgr B2 with an absorbed power-law model and two Gaussian lines (after Koyama et al 2006c, *PASJ*, submitted).

radio shell discovered by Oka et al. [13]. The kinetic energy of the radio shell is a few of  $10^{52}$  erg  $s^{-1}$ , within the range of single or multiple supernova explosions.

#### 4. Discovery of a New XRN

The 6.4 keV map shows two bright regions at (2, 2) and (1, 3). One is Sgr B2, which has been already found as a strong 6.4 keV source [15], and the other is a newly discovered source Suzaku J1747.7–2821.2 (M0.74–0.09). We show the background-subtracted spectra of M0.74–0.09 and Sgr B2 in figures 7 and 8. The latter is for comparison to the former new source. We simultaneously fit the FIs and BI spectra with a model of absorbed power-law plus two Gaussians near at 6.4 and 7.06 keV, which are for the  $K\alpha$  and  $K\beta$  lines of FeI. This model nicely fits the data except an excess near the 6.7 keV line in the Sgr B2 spectra. One possibility is that the 6.7 keV enhancement is a part of the new SNR candidate G0.61+0.01, because it is located in the close vicinity of Sgr B2. The other possibility is that the 6.7 keV enhancement is due to high mass young stellar objects (YSO) embedded in the center of Sgr B2, because some of the YSOs shows a hint of the 6.7 keV line emission [19].

The Sgr B2 cloud has been studied extensively with *ASCA* and *Chandra* [15],[17]. The authors concluded that the 6.4 keV emission is due to a fluorescent by strong X-rays coming from Sgr A\*, hence named the X-ray Reflection Nebula (XRN). *Suzaku* found a clear  $K\beta$  line at 7.06 keV of the  $\sim 10\%$  of  $K\alpha$  and deep Fe edge at 7.1 keV. These discoveries provide additional supports for the XRN scenario of Sgr B2.

The spectrum of M0.74-0.09 exhibits strong 6.4 keV line with an equivalent width of 1.6 keV, 7.06 keV line and edge structure at 7.1 keV. All these lines and edge energies are consistent with being from  $K\alpha$ ,  $K\beta$  and  $K_{\text{edge}}$  of FeI. The flux of the 7.06 keV line is about 10% of that of the 6.4 keV line, which is also consistent with the fluorescent X-rays. Unlike Sgr B2, no hint of YSOs is found so far. No bright point source is found in the *Chandra* image. Therefore, the X-rays cannot be the scattering and fluorescence by embedded YSOs or any internal source. If the X-rays from Sgr B2 and M0.74–0.09 are due to the Thomson scattering and fluorescence of the same irradiating external source like Sgr A\*, then the  $N_{\text{H}}$  ratio between these sources should be same as the 6.4 keV line flux ratio. The observed  $N_{\text{H}}$  ratio and the 6.4 keV line flux is in good agreement with each other, hence supports the fluorescent scenario. Therefore the XRN scenario successfully applied to Sgr B2 can be also applied to M0.74–0.09.

The counter scenario against the XRN is that the 6.4 keV line emission is produced by the

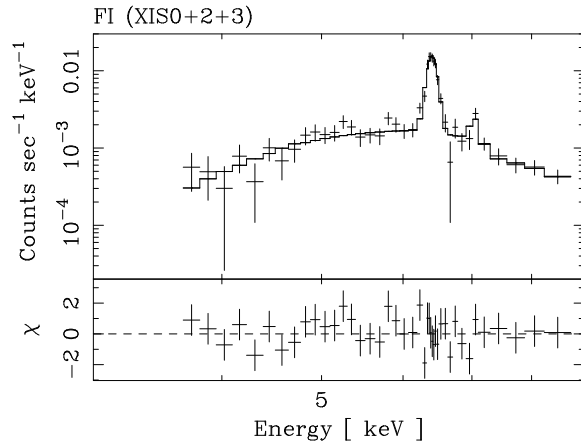


**Figure 8.** Same as figure 7, but for a new source M0.74-0.09 (after Koyama et al. 2006c, *PASJ*, submitted).

collision of electrons with neutral iron. Since the cross section of iron K-shell ionization is maximum at the electron energy of a few 10 keV [18], the most probable source is low energy electrons (LEE) as proposed for the origin of the Galactic Ridge iron K-shell emission [19]. Since a few 10 keV electrons is absorbed in less than  $10^{22} \text{H cm}^{-2}$  of depth [18], the produced X-ray spectrum has no large absorption edge. Our observation, however, shows clear absorption of  $(4-10) \times 10^{23} \text{H cm}^{-2}$ , in far excess to the Galactic interstellar absorption [12]. Thus the LEE origin is unlikely, unless we assume a special geometry such that the 6.4keV source is deep in or behind the dense cloud.

### Acknowledgments

The authors express sincere thanks to all the *Suzaku* team members and our Laboratory colleagues. Y.H. and H.N. are supported by JSPS Research Fellowship for Young Scientists. This work is supported by the Grant-in-Aid for the 21st Century COE "Center for Diversity and Universality in Physics" from the Ministry of Education, Culture, Sports, Science and Technology (MEXT) of Japan.

### References

- [1] Mitsuda, K., et al. 2006, *PASJ*, submitted
- [2] Koyama, K., et al. 2006a, *PASJ*, submitted
- [3] Serlemitsos, P. et al. 2006, *PASJ*, submitted
- [4] Kelly et al. 2006, *PASJ*, submitted
- [5] Koyama, K., et al. 2006b, *PASJ*, submitted
- [6] Koyama, K., et al. 2006c, *PASJ*, submitted
- [7] Kinkhabwala, A., et al. 2002, *ApJ*, **575**, 732
- [8] Beiersdorfer, P. 2003, *ARA&A*, **41**, 343
- [9] Perez, J. A., Olson, R. E., & Beiersdorfer, P. 2001, *J. Phys. B*, **34**, 3063
- [10] Wargelin, B. J., Beiersdorfer, P., Neill, P. A., Olson, R. E., & Scofield, J. H. 2005, *ApJ*, **634**, 687
- [11] Borkowski, K. J., Lyerly, W. J., & Reynolds, S. P. 2001, *ApJ*, **548**, 820
- [12] Sakano, M., Koyama, K., Murakami, H., Maeda, Y., & Yamauchi, S. 2002, *ApJ*, **138**, 19
- [13] Oka, T., Hasegawa, T., Sato, F., Tsuboi, M., & Miyazaki, A. 1998, *ApJS*, **118**, 455
- [14] Reid, M. J., Schneps, M. H., Moran, J. M., Gwinn, C. R., Genzel, R., Downes, D., & Roennaeng, B. 1988, *ApJ*, **330**, 809
- [15] Murakami, H., Koyama, K., & Maeda, Y. 2001, *ApJ*, **558**, 687
- [16] Takagi, S., Murakami, H., & Koyama, K. 2002, *ApJ*, **573**, 275



- [17] Koyama, K., Maeda, Y., Sonobe, T., Takeshima, T., Tanaka, Y., & Yamauchi, S. 1996, *PASJ*, **48**, 249
- [18] Tatischeff, V. 2002, *astro-ph/0208397*
- [19] Valinia, A., Tatischeff, V., Arnaud, K., Ebisawa, K., & Ramaty, R. 2000, *ApJ*, **543**, 733